JOURNAL OF Materials CHEMISTRY

Structures of Ti(IV)-doped α-FeOOH particles

Tatsuo Ishikawa,*[a] Hiroaki Yamashita,[a] Akemi Yasukawa,[a] Kazuhiko Kandori,[a] Takenori Nakayama[b] and Fumio Yuse[b]

[a]*School of Chemistry, Osaka University of Education, 4-698-1 Asahigaoka, Kashiwara, Osaka, 582-8582, Japan. E-mail: ishikawa@cc.osaka-kyoiku.ac.jp*
[b]*Materials Research Laboratory, Kobe Steel, LTD., 5-5 Takatsukadai 1-chome, Nishi-ku, Kobe, Hyogo, 615-2271, Japan*

Received 6th July 1999, Accepted 25th October 1999

The influence of Ti(IV) on the formation and structure of α-FeOOH particles was investigated by characterizing the coprecipitation products of Fe(III) with Ti(IV) at different atomic ratios (Ti/Fe) in the range 0–0.1. The particle width of the products increased as Ti/Fe was increased. At Ti/Fe $\geqslant$ 0.05 the crystallite size of α-FeOOH increased with increase of Ti/Fe while the XRD peaks decreased in intensity. Thermal analysis and Mössbauer spectroscopy showed that the α-FeOOH phase diminishes upon doping with Ti(IV) and that less crystalline regions composed of agglomerates of fine particles develop. EXAFS revealed that the doped Ti(IV) disturbs the nearest coordination structure surrounding Fe(III). According to N_2 adsorption, micropores are formed in the particles upon addition of Ti(IV). It is deduced from the obtained results that the addition of Ti(IV) produces double domain particles consisting of an α-FeOOH core and a porous poorly crystalline shell.

Introduction

α-FeOOH (goethite) which is a polymorph of iron(III) oxyhydroxide, is a primary component of soil and a main corrosion product of steel. This material also finds industrial usages as a coloring material and precursor of powders for magnetic memory applications. The incorporation of metal ions into α-FeOOH has received attention in environmental science since metal-substituted α-FeOOH is frequently found in the soil, bringing about soil contamination.[1] Also, the coprecipitation of metal ions with Fe(III) is a means to remove various harmful metal ions from waste water. On the other hand, a small amount of Cr , Ni and Cu is added to steels as anti-corrosive elements. The influences of these metal ions on the formation and structure of α-FeOOH which is a most stable corrosion product, have been investigated in order to elucidate the mechanism of anticorrosion by these metals. Inouye *et al.* found a marked inhibitory effect of Cu(II) on the formation of α-FeOOH and interpreted its anticorrosive character by a mechanism in which distortion of octahedra in α-FeOOH crystals induced by the Jahn–Teller effect of Cu(II) led to a dense rust layer on steel.[2] It has been reported that Cr(III) can be substituted for Fe(III) in α-FeOOH by up to 0.10 in terms of Cr/(Cr + Fe) atomic ratio, since α-CrOOH exists as the mineral bacewellite isostructural to α-FeOOH.[3] Yamashita *et al.* proposed that Cr-substituted α-FeOOH particles are related to the formation of a stable rust layer on a weathering steel exposed for 26 years.[4] Ni(II) also substitutes for Fe(III) of α-FeOOH particles up to an atomic ratio of *ca.* 0.1 without morphological change despite the different valency of Ni(II).[5] Recently, Yokoi *et al.* found that Ti exerts a significant anticorrosive action in steel for cars used in an environment containing Cl^- ions from anti-freezing agent.[6] However, the mechanism of the anticorrosion by Ti remains unclear and also the effect of Ti(IV) on the formation of iron(III) oxyhydroxides, including α-FeOOH, has been much less explored than the action of Cu(II), Ni(II) or Cr(III). The present study has been conducted to clarify the influence of Ti(IV) on the formation and structure of α-FeOOH. The α-FeOOH particles coprecipitated with Ti(IV) were characterized by various means. The results presented here will serve to provide a basic understanding of the mechanism involved not only in the anticorrosion action of Ti but also the uptake of Ti(IV) by α-FeOOH in soils.

Experimental

Materials

α-FeOOH particles were prepared by coprecipitation with Ti(IV) at a variety of atomic ratios (Ti/Fe) in the range 0–0.1 as follows. A determined quantity of a 2.0 mol dm^{-3} $Ti(SO_4)_2$ solution was added to 25 cm^3 of a 2.0 mol dm^{-3} $Fe(NO_3)_3$ solution and then the total volume of the solutions was adjusted to 50 cm^3 by adding water. The solution pH was set to 12 with 1.0 mol dm^{-3} NaOH solution under stirring. The resulting precipitates were aged in a polypropylene vessel at different temperatures of 30, 50 and 100 °C for 5 days. After the aging, the particles were filtered off, washed with water and vacuum-dried at room temperature for $>$15 h. All the used chemicals were reagent grade and supplied by Wako Pure Chemical Industries, Ltd.

Characterization

The materials formed were characterized by a variety of complementary means. Powder X-ray diffraction (XRD) was carried out on a Rigaku diffractometer using Cu-Kα radiation at 15 mA and 30 kV. The morphology of the particles was observed using a JEOL transmission electron microscope (TEM). Ti and Fe contents were determined using a Seiko induction coupled plasma spectrometer (ICP) by dissolving the samples in concentrated HCl and diluting to a preset concentration with water. Thermogravimetry–differential thermal analysis (TG–DTA) curves were obtained on a Seiko thermoanalyzer in an air stream at a heating rate of 5 °C min^{-1}. Mössbauer spectra were measured at room temperature on an Elscint spectrometer using γ-beam irradiation (0.92 GBq) from ^{57}Co dispersed in a Rh film. Extended X-ray absorption fine structure (EXAFS) spectroscopy was performed using the apparatus BL-7C at the National Laboratory for High Energy Physics (Tsukuba, Japan) at an accelerating voltage of

3.0 GeV. X-Ray absorption spectra at the Fe K-edge (7713 eV) were taken. To clarify the porous structures of the materials, the adsorption isotherms of N_2 were measured by an atomic volumetric apparatus assembled in our laboratory at the boiling point of liquid N_2. Prior to the adsorption the samples were outgassed at 100 °C for 2 h.

Results and discussion

TEM and XRD

To confirm the incorporation of Ti(IV) into the particles formed by the coprecipitation method, the Ti content of the particles produced at different Ti/Fe ratios was determined by ICP. The Ti/Fe ratios of the particles were close to those in the starting solutions, revealing that most of Ti(IV) ions added to the starting solutions are precipitated with Fe(III) to remain in the formed particles.

Fig. 1 shows TEM images of the particles formed for different atomic ratios (Ti/Fe) at 50 °C. It is seen that the particle width increases with increasing Ti/Fe ratio and at Ti/Fe $\geqslant$ 0.075 irregularly shaped particles are observed. Similar trends were obtained for particles formed at 30 and 100 °C. It is of interest that the particles grow upon substituting with Ti(IV) which has a larger valency than Fe(III). This effect of Ti(IV) is clearly distinct from those of Cu(II)[2] and Ni(II)[5] previously reported; a small amount of Cu(II) interferes with the crystal growth of α-FeOOH to make the particles amorphous at Cu/Fe $\leqslant$ 0.01 while Ni(II) does not influence the particle morphology at Ni/Fe $\leqslant$ 0.1.

Fig. 2 shows the XRD patterns of the products for different Ti/Fe ratios at 50 °C. The patterns of all the samples are characteristic of α-FeOOH (JCPDS 17-536). The diffraction peaks increase with increasing Ti/Fe ratio at Ti/Fe $\leqslant$ 0.02 while above this value they decrease and show narrowed peak width. None of the peaks shifts with an increase of Ti/Fe which indicates that the unit cell parameters of α-FeOOH do not vary by adding Ti(IV). A similar effect of Ti(IV) was seen for samples aged at 30 and 100 °C (not shown here). The crystallite sizes of the particles aged at 30, 50 and 100 °C, estimated by the Scherrer equation from the half height width of the (110) and (111) peaks, are plotted *vs.* the Ti/Fe ratio in Fig. 3. Comparing Fig. 1 and 3, the crystallite sizes are similar to the sizes of the particles implying they are single crystals. As seen in Fig. 3, the crystallite sizes increase with increasing Ti/Fe, in accord with the TEM result that the particle width is broadened by doping with Ti(IV). The crystallite sizes of samples prepared at higher temperatures are more markedly increased by doping with Ti(IV), *i.e.*, the crystal growth of α-FeOOH is enhanced at higher aging temperatures despite the presence of Ti(IV).

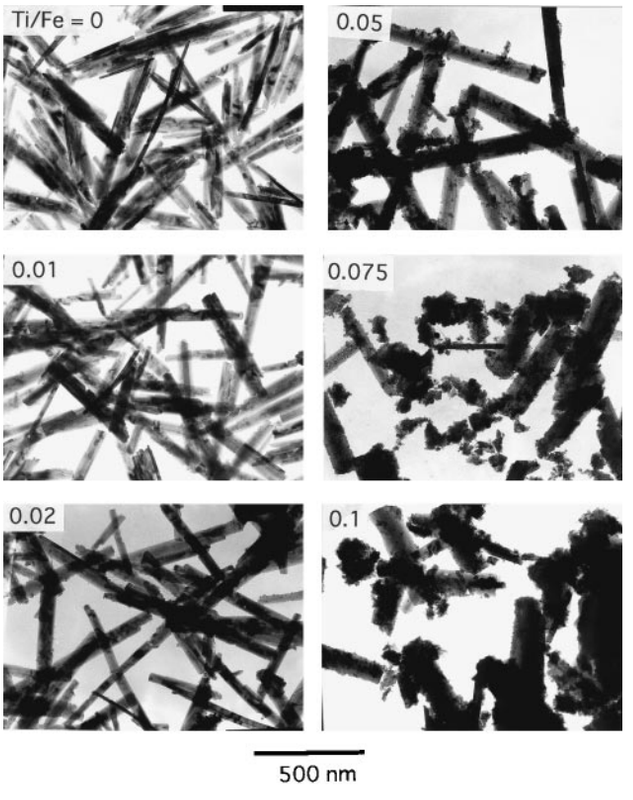

Fig. 1 TEM images of the particles formed with different Ti/Fe ratios at 50 °C.

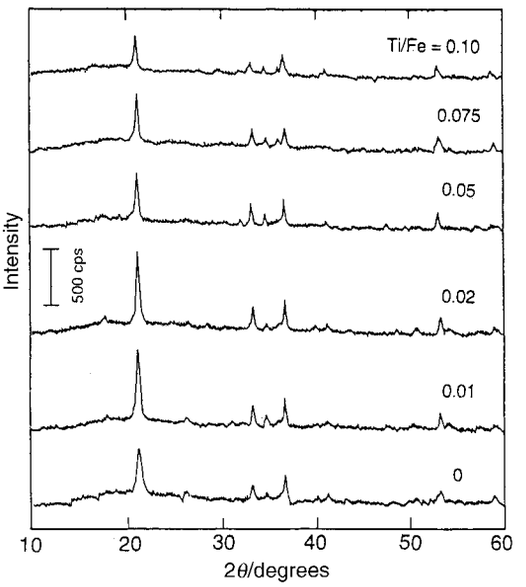

Fig. 2 XRD patterns of the particles formed with different Ti/Fe ratios at 50 °C.

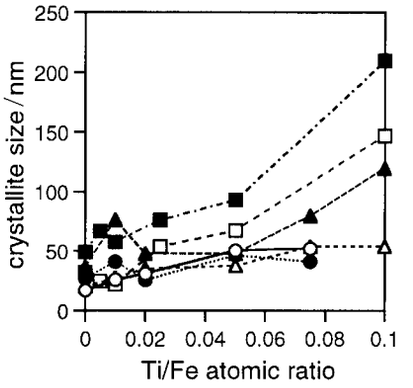

Fig. 3 Crystallite size *vs.* Ti/Fe ratio of the products at 30 (○, ●), 50 (△, ▲) and 100 °C (□, ■). The open and closed symbols refer to the crystallite sizes evaluated from the (110) and (111) peaks, respectively.

TG-DTA

Fig. 4 shows TG traces obtained for products with different Ti/Fe ratio at 50 °C. The Ti(IV)-free sample shows a steep weight loss at *ca.* 100–200 °C arising from the dehydroxylation reaction, $2FeOOH \rightarrow Fe_2O_3 + H_2O$.[7] The weight loss due to the dehydroxylation is reduced as the Ti/Fe ratio increases, while slow weight loss initiating from room temperature is noticeable for the samples prepared at Ti/Fe $\geqslant$ 0.05. This weight loss at low temperature is ascribed to the release of hydration water and/or strongly adsorbed water that would be present in less crystalline regions of the particles rather than dehydroxylation of α-FeOOH. These TG results indicate that the α-FeOOH content of the particles is reduced upon increasing

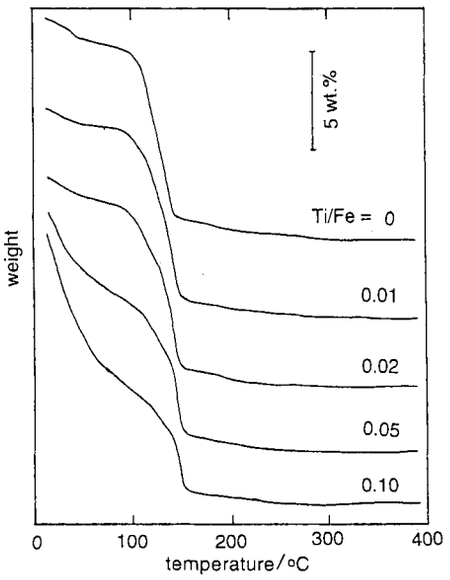

Fig. 4 TG curves of the particles formed with different Ti/Fe ratios at 50 °C.

the Ti/Fe ratio, in agreement with the XRD result that the α-FeOOH peaks of the samples produced at Ti/Fe $\geqslant$ 0.05 are weakened with increasing Ti/Fe ratio. On increasing the preparation temperature of the samples, the weight loss due to the release of water from the less crystalline regions of the sample was decreased while the weight loss due to dehydroxylation of α-FeOOH was increased (TG curves not shown). This can be attributed to crystallization of α-FeOOH at higher temperature.

The differential TG (DTG) curves obtained by differentiating the TG curves in Fig. 4 are illustrated in Fig. 5 (solid lines) along with the DTA curves (dashed lines). The DTG and DTA curves of the samples without Ti(IV) give rise to four peaks and four endothermic signals, respectively, though no clear step could be detected in the TG curves in Fig. 4. Note that the peak temperatures of DTG are identical to those of DTA, which

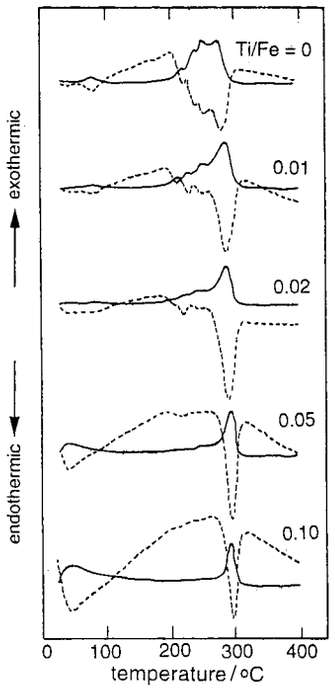

Fig. 5 DTG (—) and DTA (---) traces of the particles formed with different Ti/Fe ratios at 50 °C.

reveals that the dehydroxylation of α-FeOOH takes place *via* four steps. It is interesting that both the DTG and DTA curves of the samples formed without Ti(IV) at 30, 50 and 100 °C show, respectively, three, four and five peaks (curves of the samples prepared at 30 and 100 °C not shown). The number of the peaks in DTG and DTA is decreased by increasing the Ti/Fe ratio and both DTG and DTA traces of samples prepared at Ti/Fe $\geqslant$ 0.05 show only a single peak at higher temperature. Thus, more highly crystalline α-FeOOH formed at a higher ageing temperature shows more dehydroxylation peaks while the number of such peaks decreases with the formation of a less crystalline phase. To our knowledge, more than three dehydroxylation peaks had not been reported previously, although a double DTA peak due to dehydroxylation of pure α-FeOOH to α-Fe_2O_3 has been found by several investigators.[8–10] Derie *et al.* rationalized that an α-Fe_2O_3 shell formed around α-FeOOH retards the dehydration of the core,[9] while Murad reported that ground natural highly crystalline α-FeOOH shows a double DTA peak whereas the sample before grinding gives rise only to a single peak and interpreted this in terms of grinding facilitating the release of water.[11] Schwertmann reported a double peak due to dehydroxylation of well crystallized α-FeOOH that was attributed to an intermediate α-FeOOH phase with a slightly higher dehydroxylation temperature generated during heating.[10] Al-substituted α-FeOOH was also found to show a double peak, that was interpreted by the difference of dehydroxylation temperatures of Al–OH and Fe–OH.[12] However, these explanations for a double peak can not be directly used to interpret the presence of multiple peaks observed here. As is seen in the TEM images, the present samples are composed of particles with different particle sizes. Furthermore, heterogeneity in the particles such as polycrystallinity and lattice distortions and defects would be responsible for the multi-peak observation. As mentioned above, the samples formed at Ti/Fe $\geqslant$ 0.05 show a single peak at higher temperature than the multi-peak signal for α-FeOOH. This can be explained by a model in which α-FeOOH crystals are covered by a less crystalline phase which raises the dehydroxylation temperature of the α-FeOOH core.

N_2 adsorption

The porous structure of the products incorporating Ti(IV) was explored by analysis of N_2 adsorption isotherms. Fig. 6 shows the isotherms on the products with different Ti/Fe ratios at 50 °C, which belong to type II in the BDDT classification.[13] The isotherms on the samples prepared at Ti/Fe $\geqslant$ 0.075 steeply rise at low relative pressure (p/p_0), inferring the existence of micropores in these samples. Similar isotherms were observed for the samples aged at 30 and 100 °C (not shown here). To verify micropore formation, t-plot analysis[14] of the N_2 adsorption isotherms was carried out. Fig. 7 shows t-plots

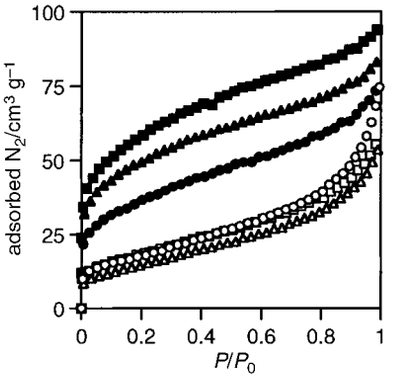

Fig. 6 Adsorption isotherms of N_2 on the products with different Ti/Fe ratios at 50 °C. Ti/Fe = 0 (○), 0.01 (△), 0.02 (□), 0.05 (●), 0.075 (▲) and 0.1 (■).

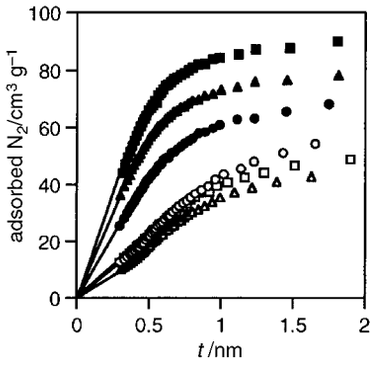

Fig. 7 t-Plots on the products with different Ti/Fe ratios at 50 °C. Ti/Fe = 0 (○), 0.01 (△), 0.02 (□), 0.05 (●), 0.075 (▲) and 0.1 (■).

obtained from the isotherms in Fig. 6. The t-plots of the samples formed at Ti/Fe ≤ 0.02 curve upwards, which indicates the formation of mesopores regarded as voids among the particles. By contrast, the t-plots of the samples formed at Ti/Fe ≥ 0.05 are bent at $t = \approx 0.5$–1.0 nm, indicating that micropores with widths of *ca.* 1–2 nm are present in the particles. Comparing the t-plots in Fig. 7 with those for the samples prepared at 30 and 100 °C (not shown here), preparation at lower temperature gives more microporous particles. The micropores in the particles are related to poorly crystalline regions formed by adding Ti(IV), since α-FeOOH itself has no micropores accessible to N_2 molecules.

To assess the microporous, less crystalline regions in the particles, the specific surface areas S_a of samples produced at different Ti/Fe ratios were evaluated using the BET equation from the N_2 adsorption isotherms. Fig. 8 shows S_a values of samples prepared at different aging temperatures *vs.* Ti/Fe. It is seen that the surface area decreases slightly with increasing Ti/Fe ratio and then steeply increases. Since the TEM result (Fig. 1) showed that the particle width is increased by doping with Ti(IV), if the particles are non-porous as presumed from the crystal structure of α-FeOOH,[15] S_a should decrease with an increase of Ti/Fe. In contradiction to this prediction, S_a values of the samples prepared at Ti/Fe ≥ 0.05 increase with increasing Ti/Fe ratio (Fig. 8). Moreover, the increase of S_a is more marked for samples prepared at lower aging temperature. It seems therefore that the increase of S_a by doping with Ti(IV) is caused by micropore formation in the poorly crystalline regions of the particles. The less crystalline regions in the particles formed at Ti/Fe ≥ 0.05 become more predominant with increasing Ti/Fe and for particles aged at lower temperature. Taking in account the TEM observations, XRD result, t-plot analysis and N_2 adsorption, the α-FeOOH crystal grows slightly upon doping with a small amount of Ti(IV) (Ti/Fe < 0.03) while at Ti/Fe ≥ 0.05 the growth of microporous, poorly crystalline regions predominates over crystal growth of α-FeOOH.

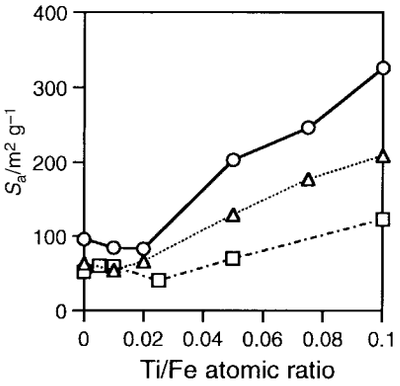

Fig. 8 Specific surface area S_a *vs.* Ti/Fe ratio of the products at 30 (○), 50 (△) and 100 °C (□).

Mössbauer spectroscopy

The above results indicate that the Ti(IV)-doped particles are composed of α-FeOOH crystals and poorly crystallized phases. Further information on the structure of the particles was obtained from Mössbauer spectroscopy. Spectra of the samples formed for varying Ti/Fe ratios at 50 °C were measured at room temperature and are shown in Fig. 9. Spectra were analyzed by least-squares fitting to a Lorenzian function. The spectrum of the product without Ti(IV) consists of a sextet assigned to the quadrupole splitting of antiferromagnetic α-FeOOH due to an inner magnetic field[16] along with two further weak sextet spectra. Thus, there are three Fe(III) sites, appearing to reflect the multidomain structure of the particles formed in the absence of Ti(IV) as suggested by TG–DTA (Fig. 5). The weak spectra do not fit the spectrum of α-Fe_2O_3[17] which exhibits a larger quadrupole splitting than that of α-FeOOH. However, the detailed origin of the weak sextet spectra is unclear at the present. As is seen in Fig. 9, with increasing Ti/Fe ratio, the α-FeOOH bands are weakened and a doublet band emerges. The spectrum of the sample formed for Ti/Fe = 0.1 shows a strong doublet band and weak α-FeOOH bands. The doublet band is usually encountered in spectra of fine paramagnetic ferric oxide particles of < *ca.* 10 nm diameter that are amorphous to XRD.[18] It is therefore clear that the Ti(IV)-doped particles contain amorphous regions which are composed of agglomerates of fine particles.

Fig. 10 shows the percentages of the area intensities of the α-FeOOH band and the doublet band as a function of the Ti/Fe ratio. With an increase of Ti/Fe ratio, the intensity of the α-FeOOH band (open circles) decreases while that of the doublet band (closed circles) increases, implying that the α-FeOOH phase diminishes and the amorphous phase is increased upon

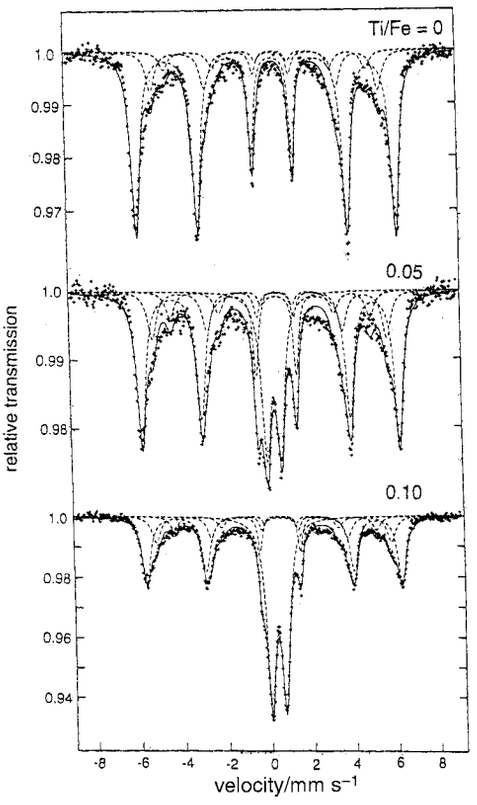

Fig. 9 Mössbauer spectra of the products with different Ti/Fe ratios at 50 °C.

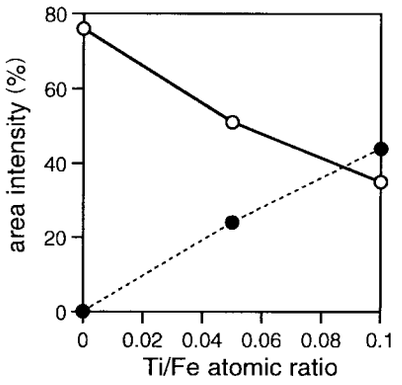

Fig. 10 Peak intensities of Mössbauer spectra *vs.* Ti/Fe ratio of the products formed at 50 °C. The open and closed circles are the intensities of sextet spectra of α-FeOOH and doublet spectra, respectively.

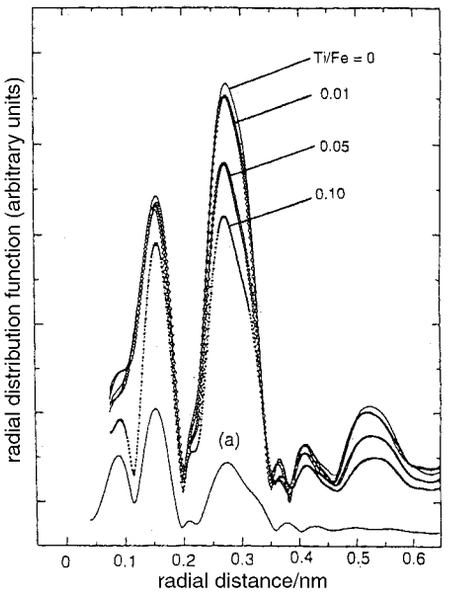

Fig. 11 Radial distribution functions of the products with different Ti/Fe ratios at 50 °C. Spectrum (a) is the function obtained for amorphous $Fe(OH)_3$ gel.

doping with Ti(IV). This Mössbauer result is thus fully in accord with the results obtained using other techniques.

EXAFS

Most of the results presented so far are indicative of the formation of a poorly crystalline phase in the particles upon doping with Ti(IV). To obtain further information on the structure of less crystalline regions, we performed EXAFS which is more sensitive to the local structure around Fe(III) than the other techniques employed in the present study. Fig. 11 depicts the radial distribution functions obtained for samples prepared with a variety of Ti/Fe ratios at 50 °C. All the functions possess two strong peaks at $R=0.15$ and 0.27 nm that are assigned to Fe–O and Fe–Fe, respectively, of edge-sharing octahedra.[19–21] The Fe–Fe peak at 0.27 nm has a shoulder to higher distance corresponding to Fe–Fe of corner-sharing octahedra. The intensity of the 0.27 nm peak (Fe–Fe) is reduced with increasing Ti/Fe ratio while the 0.15 nm peak (Fe–O) is essentially unchanged, *i.e.*, upon doping, the octahedra are separated. This indicates that Ti(IV) disarranges the orientation of octahedra in α-FeOOH crystals to produce less crystalline regions. The 0.15 nm peak (Fe–O) also contains a shoulder at <0.15 nm. As the Ti/Fe ratio is increased, this shoulder becomes distinct and is observed as a peak at $R=0.09$ nm. This peak can be ascribed to an Fe–O coordinate bond between hydration water and Fe(III) upon comparison with amorphous $Fe(OH)_3$ gel [Fig. 11(a)].

Conclusion

Based on the information presented above, it can be inferred that Ti(IV) interferes with the crystallization of α-FeOOH and the formed particles have a double domain structure composed of crystalline and amorphous phases. The core of the particles is crystalline α-FeOOH while their outer shells are composed of microporous agglomerates of ultrafine particles. The double domain particles are thought to grow in amorphous $Fe(OH)_3$ gels coprecipitated with Ti(IV) in the following process. The nuclei of α-FeOOH crystals first evolve and grow by aging *via* adsorption and crystallization of solute species on the α-FeOOH nuclei. However, Ti(IV) coprecipitated in the amorphous gels obstructs the crystallization on the surface of α-FeOOH crystal whereby the α-FeOOH crystals are covered by a less crystalline phase so that double domain particles are produced.

Acknowledgements

The authors are grateful to Mr Masao Fukusumi of Osaka Municipal Technical Research Institute for help with the TEM observations. This study was partly supported by the Grant-in-Aid for Science Research Fund (C) from the Ministry of Education, Science, Sports and Culture, Japanese Government.

References

1 J. Gerth, *Geochim. Cosmochim. Acta*, 1990, **54**, 363.
2 K. Inouye, S. Ishii, K. Kaneko and T. Ishikawa, *Z. Anorg. Allg. Chem.*, 1972, **391**, 86.
3 U. Schwertmann, U. Gasser and H. Sticher, *Geochim. Cosmochim. Acta*, 1989, **53**, 1293.
4 M. Yamashita, H. Miyuki, H. Nagano and T. Misawa, *Zairyo-to-Kankyo* (*Corrosion Engineering*), 1994, **43**, 26.
5 T. Ishikawa, A. Nagashima and K. Kandori, *J. Mater. Sci.*, 1991, **26**, 6231.
6 T. Yokoi, S. Takeuchi, H. Shirasawa and T. Nakayama, *Proceedings of the International Symposium on Plant Aging and Life, JSCE and NACE*, Sapporo, 1995.
7 R. M. Cornell and U. Schwertmann, *The Iron Oxides*, VCH, Weinheim, 1996, p. 351.
8 M. H. Creer, J. B. C. Hardy, H. P. Rooksby and J. E. Still, *Clay Miner.*, 1971, **9**, 23.
9 R. Derie, M. Ghodsi and C. Calvo-Roche, *J. Therm. Anal.*, 1976, **9**, 435.
10 U. Schwertmann, *Thermochim. Acta*, 1984, **78**, 39.
11 E. Murad, *Miner. Mag.*, 1979, **43**, 355.
12 M. V. Fey and J. B. Dixon, *Clays Clay Miner.*, 1981, **29**, 91.
13 K. S. W. Sing, D. H. Everett, R. A. W. Haul, L. Moscou, R. A. Pierotti, J. Rouquerol and T. Siemieniewska, *Pure Appl. Chem.*, 1985, **57**, 1739.
14 B. C. Lippens and J. H. de Boer, *J. Catal.*, 1965, **4**, 319.
15 C. F. Sampson, *Acta Crystallogr., Sect. B*, 1969, **25**, 1683.
16 E. Murad, *Am. Mineral.*, 1982, **67**, 1007.
17 E. Murad and U. Schwertmann, *Clays Clay Miner.*, 1986, **34**, 1.
18 R. M. Cornell and U. Schwertmann, *The Iron Oxides*, VCH, Weinheim, 1996, p. 118.
19 A. Manceau and J. M. Combes, *Phys. Chem. Miner.*, 1988, **15**, 283.
20 K. Kaneko, N. Kosugi and H. Kuroda, *J. Chem. Soc., Faraday Trans. 1*, 1989, **85**, 869.
21 J.-Y. Bottero, A. Manceau, F. Villieras and D. Tchoubar, *Langmuir*, 1994, **10**, 316.

Paper a905433b